

Article

# Application of Uniform Design Method in the Optimization of Hydrothermal Synthesis for Nano MoS<sub>2</sub> Catalyst with High HDS Activity

Haiping Zhang <sup>1,2</sup>, Hongfei Lin <sup>2</sup> and Ying Zheng <sup>2,3,\*</sup>

<sup>1</sup> Collaborative Innovation Center of Chemical Science and Engineering (Tianjin), Department of Chemical Engineering and Technology, Tianjin University, Tianjin 300072, China; hpzhang@tju.edu.cn

<sup>2</sup> Department of Chemical Engineering, University of New Brunswick, Fredericton, NB E3B 5A3, Canada; linhongfei@hotmail.com

<sup>3</sup> Department of Chemical and Biochemical Engineering, Western University, London, ON N6A 5B9, Canada

\* Correspondence: yzheng@unb.ca or ying.zheng@uwo.ca; Tel.: +1-519-661-2111

Received: 24 October 2018; Accepted: 8 December 2018; Published: 12 December 2018



**Abstract:** The optimization of catalyst synthesis conditions using traditional single factor method involves extensive experimental time and costs. To overcome the drawbacks, a uniform design method was applied in the hydrothermal synthesis of nano MoS<sub>2</sub> catalyst. An optimal synthesis condition is reached with only a few trials. Catalyst synthesis temperature is reduced to 200 °C. The catalyst synthesized at the screened condition shows high hydrotreating activities. The results conclude that the catalyst has thread-like slabs with a lattice structure that is less mature than fully developed MoS<sub>2</sub>. The characterization results indicate that the appearance of such structure may be due to the weak links of successive MoS<sub>2</sub> nuclei. The high catalytic activity is a result of the layered structure and a significantly large number of defects on the slabs.

**Keywords:** uniform design; MoS<sub>2</sub>; hydrothermal; hydrodesulfurization; low temperature

## 1. Introduction

Two-dimensional (2D) materials have historically been one of the most extensively studied classes of materials [1–3]. The discovery of single-layer graphene in 2004 by Novoselov and Geim has led to a paradigm for the investigation of novel 2D materials and their physical properties [4]. MoS<sub>2</sub> has nano-crystalline structures with stacked slabs and various morphologies [5,6], and is one of the well-studied families that have shown extraordinary optical, electrical, and mechanical properties [7,8]. Beyond, MoS<sub>2</sub> has been a widely used hydrotreating catalyst for upgrading petroleum oil in refineries [9–11].

The synthesis of MoS<sub>2</sub> by hydrothermal technique has gained great interests, due to the high quality of product and easy control of operating conditions [12–15]. It has been reported that the properties of MoS<sub>2</sub> can be influenced by a large number of factors, e.g., the concentration of precursors, pH values, reaction temperature and time, heating rate, stirring speed, etc. [16–18]. Interaction also exists among the factors. To efficiently investigate these factors and quickly screen for the optimal combination of the parameters, a proper experimental design is of great importance.

Different experimental strategies are available, e.g., factorial design. Factorial design is a commonly used design method for catalyst synthesis [19]. However, the sample size grows exponentially in the number of factors, and a huge amount of experiments are expected with multiple factors and levels ( $\geq 5$ ) [20,21]. Uniform design (UD), on the other hand, is characterized as small sample size, which accommodates the largest number of levels with fewest experimental runs among all the design methods [22,23]. The other advantage is high representativeness of trials

in the studied experimental domain. The successful application of this methodology has been well documented in many fields [24,25]. For instance, through the usage of uniform design, Li, et al. succeeded in establishing a significant linear relationship between deposition efficiency, oxide content, microhardness, fracture toughness and process parameters within 10 trials when preparing titanium nitride coatings [26].

The factors arranged in the uniform design are treated equally. However, among all the factors, the role of synthesis temperature is of particular interest, since it highly influences not only the catalyst quality, but the synthesis cost. In our previous studies, the hydrodesulfurization rate constant was increased by a factor of 2.4 when increasing the hydrothermal temperature from 200 to 350 °C in basic media [27]. A similar trend was observed by Yoosuk, B. et al. when preparing NiMoS by hydrothermal method. Enhancement of temperature from 300 to 375 °C led to an increase in dibenzothiophene and 4,6-dimethyldibenzothiophene conversion by 14% and 10%, respectively [17]. However, the activity increase from elevated temperature will be at the cost of high investment on equipment (high pressure resulting from high temperature) and operation [13]. Accordingly, seeking a high-activity catalyst at low synthesis temperature is of great significance. The existence of the combination effect of the factors provides the possibility to obtain a high-activity MoS<sub>2</sub> at low temperature through the cooperation with other parameters.

In the current paper, a novel hydrothermal technique was adopted for the synthesis of a nanocrystalline MoS<sub>2</sub> catalyst, using MoO<sub>3</sub> and Na<sub>2</sub>S as precursors [28]. A combination of factorial and uniform design was employed in this work to efficiently screen the high-activity hydrotreating catalysts. Firstly, a 2 to 3-level single-factor experiment was conducted to determine the proper range of factor levels to enhance the efficiency and reliability of the following experimental design. Based upon the obtained data, a uniform experimental design with seven factors and five levels for each factor was applied. The parameters considered include precursor concentration, precursor ratio (media pH), synthesis temperature and time, heating protocol, and stirring. A follow-up single-factor design was attempted consequently to search for optimal catalysts in a low temperature range of 160–270 °C when other parameters were fixed at the optimal conditions. To understand the mechanism of the high-activity of catalysts prepared at low temperature, a comparative analysis was conducted on the selected catalyst, in comparison to a reference MoS<sub>2</sub> with similar activity synthesized at a higher temperature (320 °C).

## 2. Results and Discussion

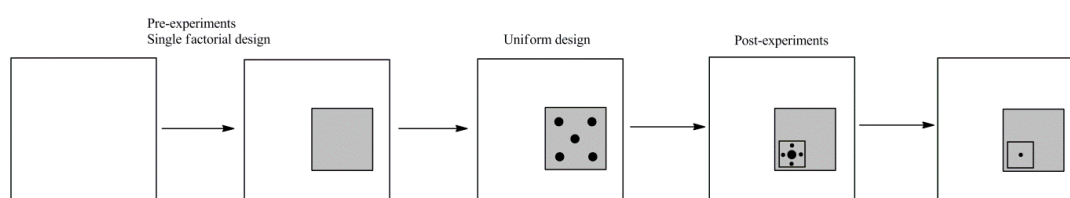
### 2.1. Screening of the Optimal MoS<sub>2</sub> Catalyst

The seeking of high hydrotreating activity catalysts involves the investigation of various factors, such as reaction temperature, pH, precursor concentration, heating rate, stirring speed, etc. Moreover, the interaction among these factors should be taken into consideration, which may result in significantly large experimental attempts. In order to efficiently screen the catalysts with fewer trails, uniform design combined with two single factorial designs was applied in this paper. As shown in Scheme 1, a series of single factorial design runs with 2–3 levels for each factor were first conducted to identify the testing window of factors. Within the selected experimental domain, uniform-design runs with high representativeness of the field were carried out for quick seeking for highly active catalysts. A further search in a narrowed area around the screened condition was accomplished through a series of post-experiments.

The parameters and responses for the single factorial design are listed in Table 1. Seven factors that may influence the catalyst activity were taken into consideration, including three precursor parameters and four operation factors. The first order hydrotreating rate constant on a mass basis other than edge Mo was selected as a criterion to evaluate catalyst's activity, based on the previous discovery that the rate constant of MoS<sub>2</sub> synthesized was related to defect density on a mass basis, i.e. hydrogen uptake in temperature programmed reduction test (TPR) and the deviation in the S/Mo stoichiometry (i.e.,

non-stoichiometry), instead of surface area or the fraction of Mo edge atoms [29]. The hydrotreating feedstock light cycle oil (LCO) contains both easy sulfur and hard sulfur, so the hydrodesulfuration (HDS) reaction was divided into two stages (0–1 h and 1–4 h) for the varied rate constants when dealing with sulfur compounds with different difficulties. Hydrodenitrogenation (HDN) rate constant was also provided based on 4 h' reaction.

The concentration of precursors is presented as MoO<sub>3</sub> concentration. With other factors fixed, the variation of MoO<sub>3</sub> concentration from 0.21 to 0.105 mol/L does not change the HDS rate dramatically, indicating that the range is not wide enough. Considering the reverse dependency, more levels will be added on the lower-value side. Two relevant precursor ratios Na<sub>2</sub>S/MoO<sub>3</sub> and HCl/MoO<sub>3</sub>, which can influence the media acidity in a different direction, were investigated in the range of 2.5–5 and 2.25–4.5, respectively. When Na<sub>2</sub>S/MoO<sub>3</sub> is 5 even at the highest HCl/MoO<sub>3</sub> ratio (4.5), little solid catalysts were obtained. A similar phenomenon is observed with HCl/MoO<sub>3</sub> of 2.25 at lowest Na<sub>2</sub>S/MoO<sub>3</sub> level. Both situations lead to basic media, which may indicate the adequate H<sup>+</sup> is essential to the successful synthesis of MoS<sub>2</sub> catalyst. Consequently, the levels of Na<sub>2</sub>S/MoO<sub>3</sub> and HCl/MoO<sub>3</sub> for uniform design are rearranged to 2.25–4.5 and 3–5, respectively.



**Scheme 1.** Experimental design.

Four operation parameters include synthesis temperature and time, heating ramp and stirring speed. Temperature from 200 to 350 °C makes the HDS rate constant increase from 19.3 to  $45.2 \times 10^{-5} \text{ s}^{-1} \text{ g cata}^{-1}$ . This indicates that the temperature has a great effect on the HDS rate and more levels in-between and higher end are needed for the uniform design. Appropriately extending the reaction time greatly benefits the HDS reaction (#8 and #9). Additional characterization of product from #8 shows the presence of unreacted MoO<sub>3</sub>, which disappears after 15 min reaction. It is indicated that 2 h crystallization is sufficient, and more levels are supplemented in-between. HDS performance is significantly improved when the heating rate increases to 30 °C/min, which is the maximum output. Accordingly, more levels are introduced below the maximum capacity of the instrument. The effect of agitation is reflected by catalysts prepared from stirring and static reactions (#1 and #3). The enhancement of the activity by stirring requires more levels of higher mixing energy. Complementary level of 100 rpm is also added to present the low stirring level on the assumption that small agitation may exert a large effect to the static reaction.

Through the screening of the parameter ranges, five levels for each factor were selected within the corresponding upper and lower boundaries. The total number of experiments for the uniform design equals the level number. A  $U_5(5^7)$  table was calculated mathematically and listed in Table 2. The significance of each factor and the reaction rate constants for each run are provided. The significance of each factor was defined as the average of relative variation of HDS activity between adjacent levels of the corresponding factors (Equation (1)). The factor levels are ordered from the smallest to the largest, and normalized by dividing their medium value.

$$S_i = \text{Average} \left( \left| \frac{\text{HDS}_{j+1,i} - \text{HDS}_{j,i}}{L_{j+1,i} - L_{j,i}} \right| \right)_{j=1-4} \quad (1)$$

where  $S_i$  denotes the significance of factor  $i$ ;  $j, j + 1$  are adjacent levels after the levels were ordered from the smallest to the largest;  $L_{j,i}$  is the dimensionless value of  $j$  level of factor  $i$  normalized upon the value of middle level (3rd level of 5 levels);  $\text{HDS}_{j,i}$  is the initial HDS rate constant on  $j$  level of factor  $i$ .

**Table 1.** Factors and responses of 2–3 level single factorial design.

Run	Factors						Responses			
	[MoO <sub>3</sub> ] (mol/L)	Na <sub>2</sub> S/MoO <sub>3</sub>	HCl/MoO <sub>3</sub>	Synthesis Temperature (°C)	Heating Rate <sup>1</sup> (°C/min)	Synthesis Time (h)	Stirring Speed (rpm)	k <sub>HDS(0–1h)</sub> <sup>2</sup> (×10 <sup>−5</sup> s <sup>−1</sup> g cata <sup>−1</sup> )	k <sub>HDS(1–4h)</sub> <sup>2</sup> (×10 <sup>−5</sup> s <sup>−1</sup> g cata <sup>−1</sup> )	k <sub>HDN(0–4h)</sub> <sup>2</sup> (×10 <sup>−5</sup> s <sup>−1</sup> g cata <sup>−1</sup> )
#1	0.105	3.75	4.5	200	3	2	500	19.3	8.1	3.2
#2	0.21	3.75	4.5	200	3	2	500	17.2	6.7	2.8
#3	0.105	3.75	4.5	200	3	2	0	15.8	5.3	2.6
#4	0.105	3.75	4.5	320	3	2	500	28.6	9.4	15.5
#5	0.105	2.5	4.5	320	3	2	500	35.1	9.7	29.3
#6	0.105	5	4.5	320	3	2	500	- <sup>3</sup>	-	-
#7	0.105	2.5	2.25	320	3	2	500	- <sup>3</sup>	-	-
#8	0.105	3.75	4.5	320	30	0	500	34.5	10.4	22.8
#9	0.105	3.75	4.5	320	30	2	500	54.9	12.5	47.0
#10	0.105	3.75	4.5	350	3	2	500	45.2	9.3	30.0

<sup>1</sup>: Average heating rate = (synthesis temperature-room temperature)/heating time. <sup>2</sup>: k<sub>HDS</sub> and k<sub>HDN</sub> were calculated based on 1st order kinetics. <sup>3</sup>: Little catalysts were generated. Hydrotreating performance test cannot be conducted due to the inadequate solid.

**Table 2.** Factors and responses of uniform experimental design.

Catalysts	CAT-1	CAT-2	CAT-3	CAT-4	CAT-5	S
[MoO <sub>3</sub> ] (mol/L)	0.0525	0.42	0.105	0.21	0.02625	0.17
Na <sub>2</sub> S/MoO <sub>3</sub>	3.75	3	4.5	2.5	2.25	0.91
HCl/MoO <sub>3</sub>	4.5	3	5	3.5	4	0.92
Temperature (°C)	340	372	270	320	200	1.15
Synthesis time (h)	0.25	0.5	0	2	1	0.26
Ave. heating rate (°C/min)	1.5	5	30	12	3	0.29
Stirring (rpm)	100	0	2000	500	1000	0.22
k <sub>HDS(0–1h)</sub> (×10 <sup>−5</sup> s <sup>−1</sup> g cata <sup>−1</sup> )	38.1	29.6	18.3	22.1	39.3	-
k <sub>HDS(1–4h)</sub> (×10 <sup>−5</sup> s <sup>−1</sup> g cata <sup>−1</sup> )	11.4	5.8	6.2	6.8	15.5	-
k <sub>HDN(0–4h)</sub> (×10 <sup>−5</sup> s <sup>−1</sup> g cata <sup>−1</sup> )	32.2	2.6	3.1	6.8	26.6	-
X <sub>S</sub> (%)	78.96	63.77	55.08	60.28	84.28	-
X <sub>N</sub> (%)	92.22	18.42	21.92	41.75	87.89	-

From Table 2, it is found that the significance of temperature is highest among all factors, which means the catalytic activity is more sensitive to temperature than others.  $\text{Na}_2\text{S}/\text{MoO}_3$  and  $\text{HCl}/\text{MoO}_3$  ratios are another two factors which greatly influence the catalytic performance, and their effects are discussed elsewhere [29]. Comparing the five catalysts, CAT-5 possess higher HDS conversion of 84.28%. It is worth noting that CAT-5 was synthesized at 200 °C, the lowest temperature in the tested range. On the other hand, CAT-2 at highest preparation temperature shows a low Sulfur conversion. It was reported that elevated temperature in hydrothermal synthesis could enhance the catalyst performance when other factors were fixed [17,27]. The current result provides an insight that low synthesis temperature can also obtain a high HDS activity by the proper combination of other factors.

A series of follow-up tests were conducted in a low temperature range of 160 to 270 °C around 200 °C (CAT-5) for the best combination of temperature with other parameters. Catalysts are denoted as CAT-6 to CAT-9 starting from lower synthesis temperature. Experimental results are shown in Figure 1. When temperature decreases to 180 and 160 °C, the S and N conversions drop dramatically. This indicates that there is a limitation for the temperature, under which the catalytic performance is not maintained. On the other side, increasing temperature to 230 and 270 °C slightly improves the activity of catalysts. However, the increase in activity is not significant and the elevated temperature will increase the operating cost and requirement on equipment. Overall considered, CAT-5 gives the highest superiority among all the prepared catalysts.

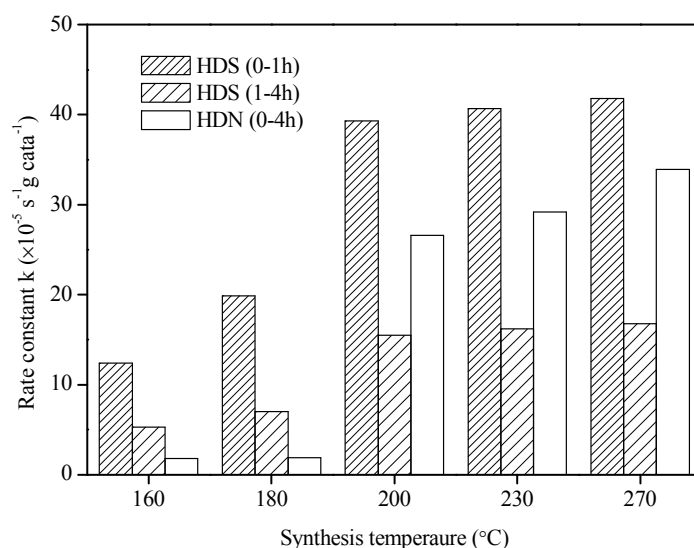


**Figure 1.** Hydrotreating activity of  $\text{MoS}_2$  catalysts.

## 2.2. Characterization of the Optimal $\text{MoS}_2$ Catalyst

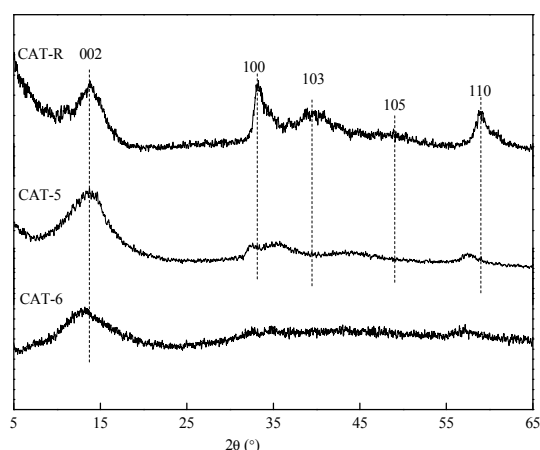
The high hydrotreating performance is derived from a catalyst synthesized at a low hydrothermal temperature. To figure out the specificity of the catalysts, a comprehensive characterization in term of crystallinity and morphology was conducted in comparison to a reference catalyst (denoted as CAT-R, Run #5 in Table 1) synthesized at a higher temperature of 320 °C using the same hydrothermal technique, which possesses a comparable HDS and HDN conversion of 76.37% and 90.20% after 4 h' hydrotreating. The reaction rate constants are listed in Table 3. According to factors' significance (Table 2), catalytic activity is most sensitive to temperature among the investigated factors. The high significance of factors  $\text{HCl}/\text{MoO}_3$  and  $\text{Na}_2\text{S}/\text{MoO}_3$ , as well as the large difference in  $\text{MoO}_3$  concentration between the selected two catalysts, may balance the effect of temperature, making these two catalysts of different synthesis temperatures both presenting high hydrotreating activity.

**Table 3.** Rate constants of MoS<sub>2</sub> catalysts.

Catalysts	Rate Constant Based on Catalyst Mass ( $\times 10^{-5} \text{ s}^{-1} \text{ g cata}^{-1}$ )			Rate Constant Based on Mo <sup>1</sup> ( $\times 10^{-2} \text{ s}^{-1} \text{ mol Mo}^{-1}$ )		
	HDS(0–1 h)	HDS(1–4 h)	HDN(0–4 h)	HDS(0–1 h)	HDS(1–4 h)	HDN(0–4 h)
CAT-5	39.3	15.5	24.4	6.1	2.4	3.8
CAT-R	35.1	9.7	29.3	5.4	1.5	4.5

<sup>1</sup>: The calculation is based on the catalysts' formula, CAT-5 of MoS<sub>1.82</sub>, CAT-R of MoS<sub>1.85</sub>.

The crystal structure of catalysts is revealed by the XRD spectra in Figure 2. CAT-R exhibits a typical crystalline MoS<sub>2</sub> spectrum, demonstrated by the characterized peaks for (002), (100), (103), and (110) Bragg planes. This indicates that MoS<sub>2</sub> phase is formed at 320 °C. For CAT-5, the intensities of the peaks are significantly weaker than those of CAT-R except the peak at 13.8°. Besides, the positions of the peaks shift left, which indicates that the layered structure is distorted. In order to distinguish the difference between the two catalysts, the interplanar spacing (*d* value), which is the perpendicular distance between successive planes, were calculated based on the XRD spectra. Table 4 summarizes the *d* values of the main Bragg planes of CAT-5 and CAT-R. It is noticed that the *d* values of (002) plane are similar for the two catalysts, which suggests that the interplanar spacing between the slabs is the same. The main differences are manifested by the *d* values of the planes (100), (103) and (110), which are enlarged from 2.695 Å, 2.260 Å and 1.564 Å to 2.758 Å, 2.513 Å to 1.605 Å, respectively. This indicates that crystalline MoS<sub>2</sub> structures are not fully generated for CAT-5. Mo atoms on the slab are not yet tightly bonded so the interplanar spacing relevant to the Mo-Mo distance is all enlarged. The low synthesis temperature may not be able to provide sufficient energy for nuclei to overcome a potential barrier to move to the proper crystal lattice. Thus, the small nuclei are gathered to form sheet-like slabs, but Mo-Mo bonds between successive nuclei particles are significantly weakened. The average length of the crystalline domains was calculated based on the plane of (110) and the results for the two catalysts are listed in Table 4. CAT-5 exhibits a smaller size of the crystalline domain than CAT-R, which also indicates CAT-5 has less ordered lattices in the catalyst.

**Figure 2.** XRD spectra of MoS<sub>2</sub> catalysts.**Table 4.** *d* values (Å) and  $\tau$  of MoS<sub>2</sub> catalysts.

Catalysts	<i>d</i> Values (Å)				$\tau$ (nm)
	(002)	(100)	(103)	(110)	Based on (110)
CAT-5	6.432	2.758	2.513	1.605	3.4 ± 0.2
CAT-R	6.421	2.695	2.260	1.564	4.1 ± 0.3

The variation of crystal structure can also be verified from XAFS results from chemical state and coordination numbers. The overall view of S K-edge and Mo L<sub>3</sub>-edge of XANES profiles are shown in Figure 3. CAT-R exhibits almost identical spectrum with reference MoS<sub>2</sub>, which confirms its crystalline structure. For CAT-R, the white line for S K-edge can be observed at 2471 eV, which represents the dominated transition of S from 1s band to 3p band [29]. The two broader peaks at 2479 eV and 2490 eV can be interpreted as the S-Mo pyramidal coordination and S hexagon structure. CAT-5 has the white line similar to CAT-R, but the amplitude of S K-edge is much lower (similar peak area, due to the broadening effect). The broadened peak may be due to the existence of other oxidation states of S. The peak position slightly shifts to higher energy, indicating that the S oxidation state on CAT-5 is increased and the local electron density on S atom is decreased. As the consequence, the structure of the pyramid should be rearranged with the electron transfer from S atom to Mo atom. Moreover, a small shoulder is shown on the onset of the white line of CAT-5, which maybe attribute to the appearance of new inner electron orbital resulting from the change of S coordination. A significant difference between CAT-5 and CAT-R is the absence of the second structural peak of MoS<sub>2</sub> (2490 eV). This probably indicates the weakness of S hexagon structure on the basal plane. The white line for Mo L<sub>3</sub>-edge is found at 2524 eV, which is associated with the electron transition from 2p<sub>3/2</sub> to vacant 4d level [30,31]. The peak located at 2532 eV represents the Mo trigonal prismatic coordination [30,32]. It is revealed that the white line for the two catalysts is almost identical, which is probably due to the high stability of Mo 4d electronic state. However, the structural characteristic peak shifts to higher energy, which is consistent with the observation from S K-edge.

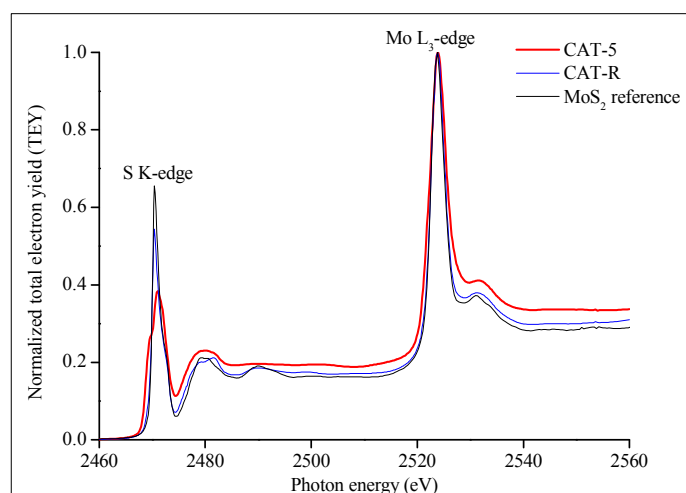


**Figure 3.** XANES spectra of MoS<sub>2</sub> catalysts.

Figure 4 shows the Fourier transformed EXAFS spectra of Mo K-edge of CAT-5 and CAT-R. Two large peaks are revealed for CAT-R at 1.92 Å and 2.86 Å, which are assigned to Mo-S and Mo-Mo scattering, respectively. The structural parameters were calculated by curve fitting of the data in the range of  $k = 3\text{--}17 \text{ \AA}^{-1}$ , using MoS<sub>2</sub> crystal as a standard ( $R_{\text{Mo-S}} = 2.413$ ,  $R_{\text{Mo-Mo}} = 3.166$ ), as shown in Table 5. For CAT-5, Mo-S scattering is significantly reduced, which indicates the dramatic decrease of Mo-S coordination number. The Mo-S bonds also decrease by 0.01 Å. It is probably the transit state prior to the mature MoS<sub>2</sub>. It is found that the peak at Mo-Mo scattering is diminished compared to CAT-R, which suggests Mo-Mo bonds are not successfully established. Microprobe elemental analysis shows no other elements, e.g., Na, Cl, O on CAT-5, and the S/Mo atomic ratio of 1.82 is close to 2 (Table 3). XRD patterns also exhibit only one single sulfide phase. These results suggest that chemical reaction was finished and CAT-5 may be in the transit state of crystallization. Combining the XANES and EXAFS results, it is tending to conclude that the Mo framework of CAT-5 is less efficiently formed than the typical MoS<sub>2</sub>.

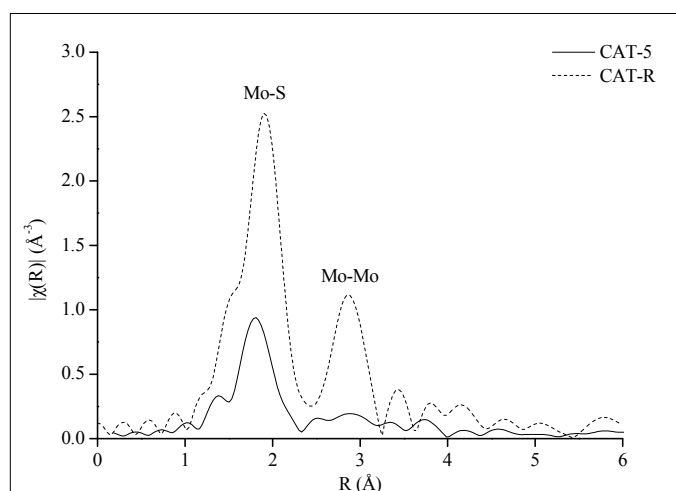


**Figure 4.** Fourier transformed EXAFS spectra of MoS<sub>2</sub> catalysts.

**Table 5.** Structural parameters resulting from the Mo K-edge Fourier-filtered k<sub>3</sub>-weighted EXAFS of MoS<sub>2</sub> catalysts.

Sample	Path	CN	R (Å)	σ <sup>2</sup> (Å <sup>2</sup> )	R <sub>f</sub>
MoS <sub>2</sub> reference	Mo-S	6	2.413	-	-
	Mo-Mo	6	3.166	-	-
CAT-5	Mo-S	2.2 ± 0.3	2.400 ± 0.015	0.005	0.0308
	Mo-Mo	-	-	-	-
CAT-R	Mo-S	5.0 ± 0.1	2.408 ± 0.003	0.002	0.0047
	Mo-Mo	4.0 ± 0.3	3.164 ± 0.004	0.004	-

Figure 5 shows the TEM images for the CAT-5 and CAT-R in different scales. It confirms the formation of stacked slabs for CAT-5, since both catalysts exhibit thread-like fringes which correspond to the 002 plane. Combined with the XRD results, it proves that the generated nuclei are linked together rather than distributing individually. Typical nanocrystalline morphology is observed from CAT-R with parallel layers and orderly edges, which is also consistent with XRD results showing a good crystal structure. Compared to CAT-R, CAT-5, on the other hand, shows a poorly crystalline morphology. As seen from the white circle on Figure 4b, a high degree of curvature, intersection and breakpoints are shown on the basal plane. This is expected since the basal is easier to be bent or broken when the Mo-Mo bond is weakened. It is also noticed that the slabs of CAT-5 are more likely to twist together, while CAT-R tends to have dispersed slabs. This likely resulted from the higher thermal movement of the catalyst under higher temperature. The average lengths of the two catalysts are listed in Table 6, which shows that the length of CAT-5 is much shorter than that of CAT-R. One possible reason is that higher temperature can benefit the formation of crystalline MoS<sub>2</sub> by enhancing the crystalline growth. Due to the shorter slab, more edge sites are generated on CAT-5.

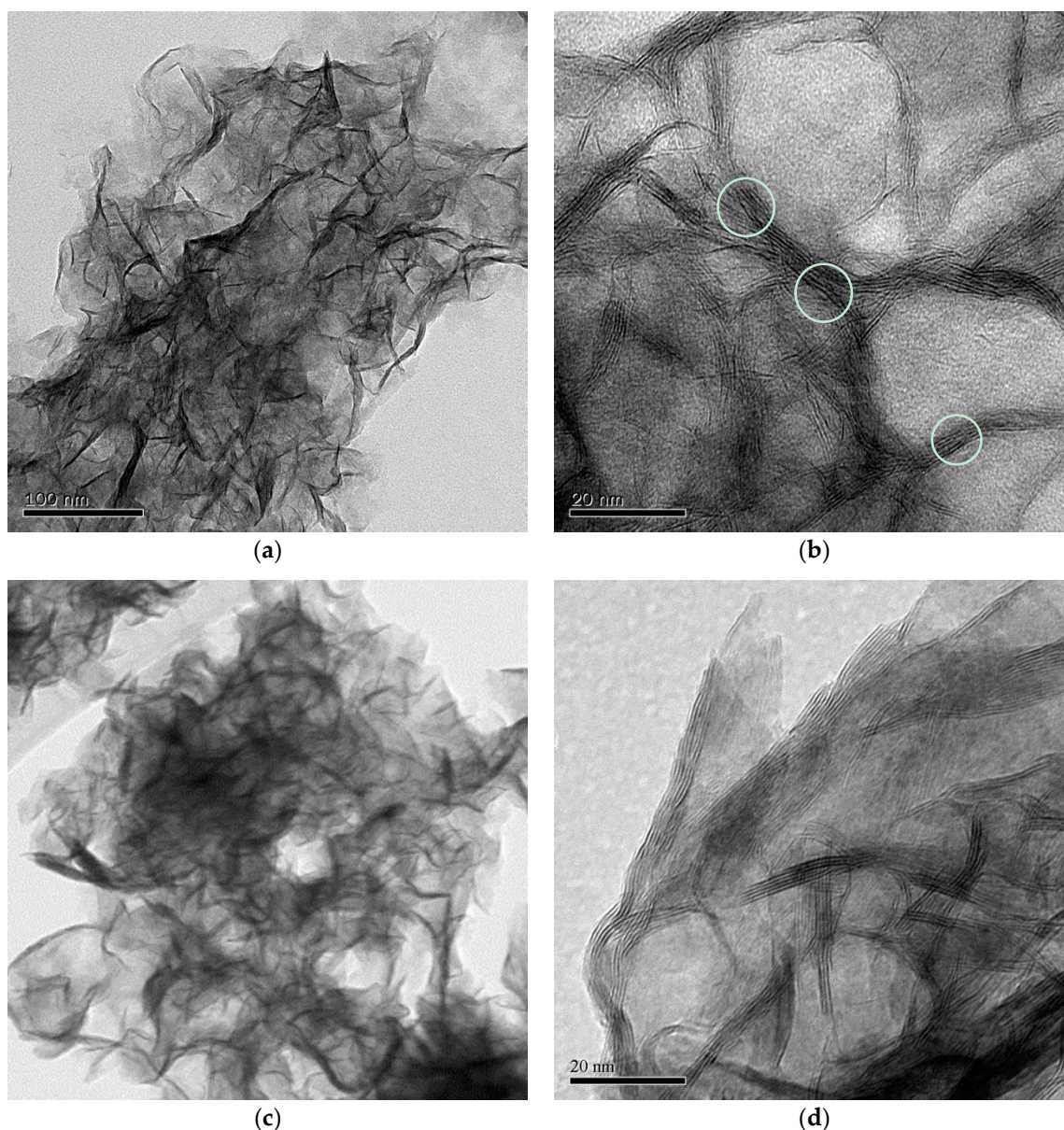


**Figure 5.** TEM images of MoS<sub>2</sub> catalysts (a,b), CAT-5; (c,d), CAT-R.

**Table 6.** Chemical composition and textural properties of MoS<sub>2</sub> catalysts.

Properties	CAT-5	CAT-R
S/Mo atomic ratio	1.82	1.85
Average Slab length (nm)	10.9	17.4
Average Slab thickness (nm)	1.7	2.9
Fraction of edge sites <sup>1</sup>	0.111	0.071
BET surface area (m <sup>2</sup> /g)	105.1	236.3
Total pore volume (cm <sup>3</sup> /g)	0.221	2.276

<sup>1</sup>: Fraction of edge Mo atoms in total Mo atoms in the slab calculated based on TEM images.

The isotherm curves of CAT-5 and CAT-R at 77 K are shown in Figure 6. For CAT-R, the adsorption curve exhibits a linear profile with a low slope when the  $P/P_0$  is below 0.8, implying a weak adsorption force between the catalyst surface and nitrogen molecule. When the  $P/P_0$  is higher than 0.7, the adsorption volume increases dramatically with the increase of pressure. This indicates the occurrence of capillary attraction and condensation. The hysteresis loop shown on CAT-R is associated

with the cylindrical pores. For CAT-5, the linear feature ends up at the same  $P/P_0$  ratio with CAT-R. Compared to CAT-R, CAT-5 has a weaker capillary phenomenon and adsorption tends to saturate after  $P/P_0 = 0.9$  without condensation. This indicates that CAT-5 possesses dramatically higher surface free energy (or surface tension) than that of CAT-R. This is also proved by the type of hysteresis loop, which shows that plane type pores are dominated in CAT-5. The total pore volume and BET surface area of CAT-5 and CAT-R are shown in Table 6. It is revealed that CAT-5 has less total pore volume and a smaller specific surface area than CAT-R.

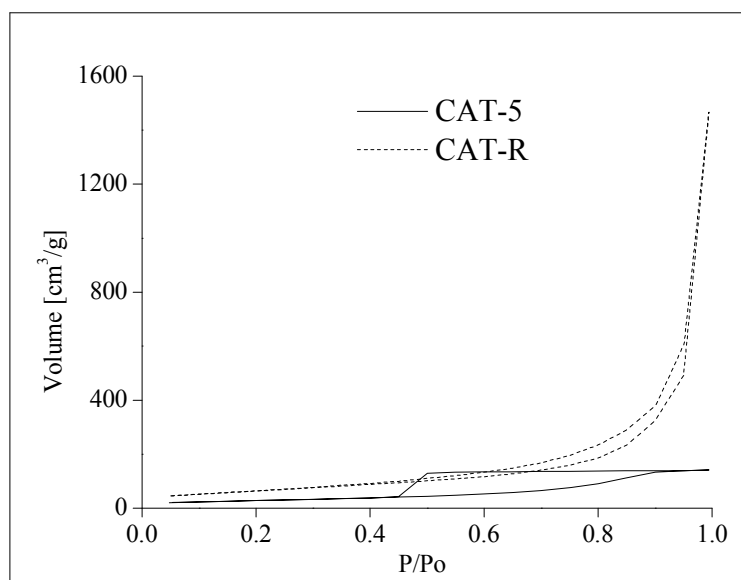


**Figure 6.** Isotherm curve of CAT-5 and CAT-R catalysts.

### 2.3. Illustration of the Reason for High Activity of the Low Temperature Synthesized Catalyst

Two catalysts CAT-5 and CAT-R (Run #5 in Table 1) synthesized at different temperature domains exhibit similar activities, but distinct properties. Their difference is mainly reflected by catalyst crystallinity and morphology. Compared to CAT-R, which is of a good crystallinity, CAT-5 shows a less developed crystalline structure with a larger number of defects.

From the catalytic view, the catalytic activity of  $\text{MoS}_2$  is originated from its crystalline structure. It is generally accepted that catalytic reaction occurs on the sites of the exterior surface of a crystal where the Mo atom is coordinatively unsaturated [33–35]. The crystal structure is essential for the generation of structural sulfur deficiency. Only the vacancies created in the lattice structure other than fully amorphous phase is capable of providing the adsorption sites for the sulfur in substances. When the majority of the material is amorphous lacking layered structure, high activity cannot be obtained, e.g., CAT-6 (Figures 1 and 2). Compared to CAT-R, CAT-5 shows a lower crystallinity, but with a layered structure maintained. The high activity of CAT-5 indicates that a low crystallinity with certain layered structure may be sufficient for providing structural active sites. On the other hand, defects on surfaces are also required for a good catalyst. Fully saturated sulfur on the straight basal plane cannot be removed to provide the adsorption sites, due to strong bonding energy. Two kinds of defect sites are responsible for the hydrodesulfurization activity, edge sites and basal defects [36–38]. Shorter slabs of CAT-5 lead to more edge sites (11.1% edge Mo for CAT-5 and 7.1% edge Mo for CAT-R). Additionally, the distorted structure brings in extensive basal defects, including curvature, breakpoint, intercrossing, etc. Thus, CAT-5 possesses more defect sites overall.

From the above analysis, the catalytic activity is related with both the crystallinity and the number of defects. Actually, these two characteristics are correlated. When the crystallinity is extremely high, the crystalline grows into large size and little defects are expected. On the other hand, the threshold

in crystallinity also exists. Without a layered structure, defects on highly amorphous phase cannot function, i.e., CAT-6. Thus, high activity can only be derived from a certain range of crystallinity, while crystalline structure and defects are both presented. The established partial crystalline structure and a large number of defects are responsible for the comparable activity of CAT-5. Compared to CAT-R, although some of the defects may not function due to the partial amorphous phase formed at 200 °C, it can be compensated by excessive defects on the layered structure. This provides a strategy for the preparation of high-performance catalysts at a lower temperature with less investment.

### 3. Experimental

#### 3.1. Uniform Design

Uniform design (UD) is one of space filling designs that the test points are uniformly distributed over the entire test range. It was first proposed by Fang and Wang in 1980s based on the quasi-Monte Carlo method or number-theoretic method [39,40]. This method can uniformly select limited representative scattered test points (experimental trials) from the comprehensive test sites to represent the whole domain. In a uniform design, there is only one trial at each level for each factor, i.e., the total number of experiments for the uniform design equals the number of levels. Its application is related to UD tables. For example, one experiment contains  $S$  factors, each factor has  $q$  levels, the  $U_n(S^q)$  table with total experimental trials of  $q$  will be applied. In this experiment, a  $U_5(5^7)$  table was employed.

#### 3.2. Synthesis Procedure

A series of molybdenum sulfide catalysts were synthesized by hydrothermal method using  $\text{MoO}_3$  (STEM Scientific, Lyndhurst, NJ, USA),  $\text{Na}_2\text{S}\cdot 9\text{H}_2\text{O}$  and  $\text{HCl}$  (Fisher Scientific, Ottawa, ON, Canada) as precursors. Single factorial design and uniform design method were applied in the work. Experimental parameters are listed in Tables 1 and 2. After each run, the resultant black solid was filtered with fine filter paper, and then washed with distilled water and ethanol (Fisher Scientific, Ottawa, ON, Canada). The final product powder was obtained from spray drying method. The prepared catalysts were denoted as CAT-Run No. in Table 2. A reference  $\text{MoS}_2$  catalyst for comparison was denoted as CAT-R.

#### 3.3. Characterization of Catalysts

The morphology of catalysts was revealed by Transmission electron microscopy (JEOL 2011 STEM, JEOL Ltd., Tokyo, Japan). The length and layer numbers of catalysts were measured using image analysis software. The fraction of molybdenum edge sites was calculated based on Gibbs–Curie–Wulf law using Equations (2)–(5) [41].

$$\text{Mo}_t = 3n^2 + 3n + 1 \quad (2)$$

$$\text{Mo}_e = 6n \quad (3)$$

$$\bar{L} = 2n \times 0.316 \quad (d_{\text{Mo-Mo}} = 0.316 \text{ nm}) \quad (4)$$

$$a = \frac{\text{Mo}_e}{\text{Mo}_t} \quad (5)$$

where  $\text{Mo}_t$  is the total number of Mo atoms in the slab;  $\text{Mo}_e$  is the number of edge Mo atoms, presumed to be catalytically active;  $n$  equals one for the smallest entity;  $a$  is the fraction of edge sites;  $\bar{L}$  is the average length determined from TEM measurements, which is the longest dimension of the hexagonal crystallites.

Nitrogen adsorption-desorption isotherm was obtained at 77K using Autosorb-1 (Quantachrome Instruments, Boynton Beach, FL, USA). The specific surface area of the catalyst powder was calculated using the Brunauer-Emmett-Teller (BET) method. The total pore volume was estimated from the volume of nitrogen adsorbed at the relative pressure  $p/p_0$  of 0.995.

The elemental analysis of catalysts was conducted on a JEOL-733 Superprobe.

The crystallinity of catalyst was characterized by powder X-ray diffraction (XRD), which was recorded on a diffractometer (Bruker AXS D8 XRD, Karlsruhe, Germany) using Cu K $\alpha$  radiation with the 2 $\theta$  range of 5–85° and the scan speed of 1°/min. The interplanar spacing (*d* value), which is the perpendicular distance between successive planes, were calculated based on the XRD spectra (Equation (6)).

$$d = \frac{n\lambda}{2 \sin \theta'} \quad (6)$$

where *d*,  $\lambda$ , and  $\theta$  denote the interplanar spacing, wavelength of the X-ray (1.5406 Å [42]), and the Bragg angle, respectively. The sizes of the crystalline domains for the catalysts were calculated by the Scherrer Equation from 110 planes (Equation (7)) [43].

$$\tau_{hkl} = \frac{K_{hkl}\lambda}{\beta_{hkl} \cos \theta'} \quad (7)$$

where  $\tau$ , *K*, and  $\beta$  denote the average size of crystalline domains, dimensionless shape factor (0.76 [43,44]), and the line broadening at half the maximum intensity, respectively.

The S K-edge and Mo L<sub>3</sub>-edge XANES of the catalysts were obtained at the Soft X-ray Microanalysis Beamline (SXRMB) of the Canadian Light Source (CLS; Saskatoon, SK, Canada) using a Si (1 1 1) double crystal monochromator. CLS, a 2.9 GeV, third generation storage ring, presently operates with an injection current of 250 mA. The measurements were made in total electron yield by recording the sample drain current. The XANES spectra were normalized to incident photon flux and to unity at the maximum intensity of each spectrum. Linear combination fitting of Mo L<sub>3</sub>-edge spectra was performed using Athena software. The fitting was performed using the first derivative curves, and the weights of the components were set to be between 0 and 1. Mo K-edge EXAFS spectra (CLS; Saskatoon, SK, Canada) were recorded at room temperature in the transmission mode. The beam intensity was measured before and after the sample (*I*<sub>0</sub> and *I*, respectively) using ionization chambers filled with mixtures of 15% Ar and 85% N<sub>2</sub> for *I*<sub>0</sub> and 50% Ar and 50% N<sub>2</sub> for *I*. Fourier transformation of EXAFS data for  $\Delta k = 14 \text{ \AA}^{-1}$  ( $3 < k < 17$ ) was performed using FEFF 6 software to obtain the structure parameters around Mo.

#### 3.4. Evaluation of Unsupported Catalysts

A batch reactor from Autoclave Engineering was employed in this experiment. A light cycle oil (LCO) with 14,600 ppm sulfur and 156 ppm nitrogen was selected as feedstock. Catalyst filtered through 200 meshes and LCO with a weight ratio of 1:200 were added into the autoclave and heated up. The hydrotreating process took place at 375 °C under 1400–1500 psi hydrogen and lasted for 4 h. The sulfur and nitrogen content in original LCO and hydrotreated products were determined by a Sulfur/Nitrogen analyzer (9000 series, Antek Instruments Inc., Houston, TX, USA). The conversion of sulfur and nitrogen was calculated using Equation (8).

$$X = \frac{C_{\text{Feed}} - C_{\text{Product}}}{C_{\text{Feed}}} \times 100\% \quad (8)$$

where *X* stands for the sulfur or nitrogen conversion; *C*<sub>Feed</sub> and *C*<sub>Product</sub> represent sulfur or nitrogen content in the feed and products. The catalytic rate constant was calculated based on the 1st order reaction. The hydrotreating experiments were repeated for three times for each catalyst, and the relative deviation of rate constant is no more than 4%.

## 4. Conclusions

The catalyst synthesized at 200 °C (CAT-5) is selected after the screening of uniform design. It is indicated that high-HDS-activity catalyst can be formed at low synthesis temperature with the proper combination of other factors. After 4 h reaction, the S and N conversion reaches 84.28% and 87.89%,

respectively. Further characterization tends to conclude that CAT-5 has a less mature structure than typical MoS<sub>2</sub>. Although thread-like slabs can be revealed, its Mo framework is not tightly formed. XRD, XANES, EXAFS, and TEM results indicate that the formation of slabs may contribute to the weak links of successive MoS<sub>2</sub> nuclei. The less mature CAT-5 contains significantly more defects than developed MoS<sub>2</sub>, which leads to a high catalytic activity.

**Author Contributions:** Conceptualization: Y.Z. and H.L.; Data curation, H.Z.; Formal analysis, H.Z.; Funding acquisition, Y.Z.; Investigation, H.Z. and H.L.; Methodology, H.Z. and H.L.; Project administration, H.L. and Y.Z.; Resources, Y.Z.; Supervision, Y.Z.; Validation, H.Z.; Writing—original draft, H.Z.

**Funding:** This research was funded by NSERC Discovery Grant, grant number RGPIN-228020-2004, Canada Foundation for Innovation, grant number 12925 and Atlantic Innovation Fund, grant number 192090.

**Acknowledgments:** The authors gratefully acknowledge the financial assistance from Natural Sciences and Engineering Research Council of Canada (NSERC), Canada Foundation for Innovation and Atlantic Innovation Fund.

**Conflicts of Interest:** The authors declare no conflict of interest.

## References

1. Novoselov, K.S.; Jiang, D.; Schedin, F.; Booth, T.J.; Khotkevich, V.V.; Morozov, S.V.; Geim, A.K. Two-dimensional atomic crystals. *Proc. Natl. Acad. Sci. USA* **2005**, *102*, 10451–10453. [[CrossRef](#)]
2. Yao, K.; Fu, Y.; Shi, L.; Wan, W.; You, X.; Yu, F. Reactive two-dimensional layered material with regular chlorine groups. *J. Colloid Interface Sci.* **2007**, *315*, 400–404. [[CrossRef](#)] [[PubMed](#)]
3. Naguib, M.; Mashtalir, O.; Carle, J.; Presser, V.; Lu, J.; Hultman, L.; Gogotsi, Y.; Barsoum, M.W. Two-Dimensional Transition Metal Carbides. *ACS Nano* **2012**, *6*, 1322–1331. [[CrossRef](#)] [[PubMed](#)]
4. Novoselov, K.S.; Geim, A.K.; Morozov, S.V.; Jiang, D.A.; Zhang, Y.; Dubonos, S.V.; Grigorieva, I.V.; Firsov, A.A. Electric Field Effect in Atomically Thin Carbon Films. *Science* **2004**, *306*, 666–669. [[CrossRef](#)] [[PubMed](#)]
5. Chianelli, R.R.; Prestridge, E.B.; Pecoraro, T.A.; DeNeufville, J.P. Molybdenum Disulfide in the Poorly Crystalline “Rag” Structure. *Science* **1979**, *203*, 1105–1107. [[CrossRef](#)] [[PubMed](#)]
6. Enyashin, A.; Gemming, S.; Seifert, G. Nanosized allotropes of molybdenum disulfide. *Eur. Phys. J. Spec. Top.* **2007**, *149*, 103–125. [[CrossRef](#)]
7. Shembel, E.; Apostolova, R.; Kirsanova, I.; Tysyachny, V. Electrolytic molybdenum sulfides for thin-layer lithium power sources. *J. Solid State Electrochem.* **2008**, *12*, 1151–1157. [[CrossRef](#)]
8. Chuang, M.-K.; Yang, S.-S.; Chen, F.-C. Metal Nanoparticle-Decorated Two-Dimensional Molybdenum Sulfide for Plasmonic-Enhanced Polymer Photovoltaic Devices. *Materials* **2015**, *8*, 5414–5425. [[CrossRef](#)]
9. Camacho-Bragado, G.A.; Elechiguerra, J.L.; Olivas, A.; Fuentes, S.; Galvan, D.; Yacamán, M.J. Structure and catalytic properties of nanostructured molybdenum sulfides. *J. Catal.* **2005**, *234*, 182–190. [[CrossRef](#)]
10. Yang, L.; Wang, X.Z.; Liu, Y.; Yu, Z.F.; Liang, J.J.; Chen, B.B.; Shi, C.; Tian, S.; Li, X.; Qiu, J.S. Monolayer MoS<sub>2</sub> anchored on reduced graphene oxide nanosheets for efficient hydrodesulfurization. *Appl. Catal. B Environ.* **2017**, *200*, 211–221. [[CrossRef](#)]
11. Guo, K.; Ding, Y.; Yu, Z.X. One-step synthesis of ultrafine MoNiS and MoCoS monolayers as high-performance catalysts for hydrodesulfurization and hydrodenitrogenation. *Appl. Catal. B Environ.* **2018**, *239*, 433–440. [[CrossRef](#)]
12. Ota, J.R.; Srivastava, S.K. A new hydrothermal route for synthesis of Molybdenum Disulphide nanorods and related nanostructures. *J. Nanosci. Nanotechnol.* **2006**, *6*, 168–174. [[CrossRef](#)] [[PubMed](#)]
13. Tian, Y.; He, Y.; Zhu, Y. Low temperature synthesis and characterization of molybdenum disulfide nanotubes and nanorods. *Mater. Chem. Phys.* **2004**, *87*, 87–90. [[CrossRef](#)]
14. Byrapp, K.; Yoshimura, M. *Handbook of Hydrothermal Technology*, 2nd ed.; William Andrew: Oxford, UK, 2013.
15. Shi, J.W.; Zhang, Y.Z.; Hu, Y.C.; Guan, X.; Zhou, Z.; Guo, L. NH<sub>3</sub>- treated MoS<sub>2</sub> nanosheets as photocatalysts for enhanced H<sub>2</sub> evolution under visible-light irradiation. *J. Alloy. Compd.* **2016**, *688*, 368–375. [[CrossRef](#)]
16. Devers, E.; Afanasiev, P.; Jouguet, B.; Vrinat, M. Hydrothermal syntheses and catalytic properties of dispersed molybdenum sulfides. *Catal. Lett.* **2002**, *82*, 13–17. [[CrossRef](#)]

17. Yoosuk, B.; Song, C.; Kim, J.H.; Ngamcharussrivichai, C.; Prasassarakich, P. Effects of preparation conditions in hydrothermal synthesis of highly active unsupported NiMo sulfide catalysts for simultaneous hydrodesulfurization of dibenzothiophene and 4,6-dimethyldibenzothiophene. *Catal. Today* **2010**, *149*, 52–61. [[CrossRef](#)]
18. Li, W.J.; Shi, E.W.; Ko, J.M.; Chen, Z.Z.; Ogino, H.; Fukuda, T. Hydrothermal synthesis of MoS<sub>2</sub> nanowires. *J. Cryst. Growth* **2003**, *250*, 418–422. [[CrossRef](#)]
19. Kleijnen, J.P.C. An overview of the design and analysis of simulation experiments for sensitivity analysis. *Eur. J. Oper. Res.* **2005**, *164*, 287–300. [[CrossRef](#)]
20. Dey, A.; Mukerjee, R. Development of Research in Experimental Design in India. *Int. Stat. Rev.* **2012**, *80*, 231–252. [[CrossRef](#)]
21. Allore, H.G.; Murphy, T.E. An examination of effect estimation in factorial and standardly-tailored designs. *Clin. Trials* **2008**, *5*, 121–130. [[CrossRef](#)] [[PubMed](#)]
22. Liang, Y.-Z.; Fang, K.-T.; Xu, Q.-S. Uniform design and its applications in chemistry and chemical engineering. *Chemom. Intell. Lab. Syst.* **2001**, *58*, 43–57. [[CrossRef](#)]
23. Fang, K.-T.; Lin, D.K.J. Ch. 4. Uniform experimental designs and their applications in industry. In *Handbook of Statistics*; Khattree, R., Rao, C.R., Eds.; Elsevier: Amsterdam, The Netherlands, 2003; pp. 131–170.
24. Zhang, S.; Chen, S.; Wang, H.; Wang, W.; Chen, Z. A model updating method for truss structure using stepwise uniform design schemes considered primary factors. *Lat. Am. J. Solids Struct.* **2014**, *11*, 19–34. [[CrossRef](#)]
25. Li, W.; Liu, L.; Gong, W. Multi-objective uniform design as a SVM model selection tool for face recognition. *Expert Syst. Appl.* **2011**, *38*, 6689–6695. [[CrossRef](#)]
26. Li, J.F.; Liao, H.; Normand, B.; Cordier, C.; Maurin, G.; Foct, J.; Coddet, C. Uniform design method for optimization of process parameters of plasma sprayed TiN coatings. *Surf. Coat. Technol.* **2003**, *176*, 1–13. [[CrossRef](#)]
27. Zhang, H.; Lin, H.; Zheng, Y.; Hu, Y.; MacLennan, A. Understanding of the effect of synthesis temperature on the crystallization and activity of nano-MoS<sub>2</sub> catalyst. *Appl. Catal. B Environ.* **2015**, *165*, 537–546. [[CrossRef](#)]
28. Zhang, H.P.; Lin, H.F.; Zheng, Y.; Hu, Y.F.; MacLennan, A. The catalytic activity and chemical structure of nano MoS<sub>2</sub> synthesized in a controlled environment. *React. Chem. Eng.* **2016**, *1*, 165–175. [[CrossRef](#)]
29. Surisetty, V.R.; Hu, Y.F.; Dalai, A.K.; Kozinski, J. Structural characterization and catalytic performance of alkali (K) and metal (Co and Rh)-promoted MoS<sub>2</sub> catalysts for higher alcohols synthesis. *Appl. Catal. A Gen.* **2011**, *392*, 166–172. [[CrossRef](#)]
30. Aritani, H.; Tanaka, T.; Funabiki, T.; Yoshida, S.; Eda, K.; Sotani, N.; Kudo, M.; Hasegawa, S. Study of the local structure of molybdenum-magnesium binary oxides by means of Mo L(3)-edge XANES and UV-vis spectroscopy. *J. Phys. Chem.* **1996**, *100*, 19495–19501. [[CrossRef](#)]
31. Zubavichus, Y.V.; Golub, A.S.; Novikov, Y.N.; Slovokhotov, Y.L.; Nesmeyanov, A.N.; Schilling, P.J.; Tittsworth, R.C. XAFS study of MoS<sub>2</sub> intercalation compounds. *J. Phys. IV* **1997**, *7*, 1057–1059. [[CrossRef](#)]
32. Aritani, H.; Fukuda, O.; Miyaji, A.; Hasegawa, S. Structural change of molybdenum on silica-alumina in contact with propene studied by ESR and Mo L-III-edge XANES. *Appl. Surf. Sci.* **2001**, *180*, 261–269. [[CrossRef](#)]
33. Kogan, V.M.; Dung, N.T.; Yakerson, V.I. Comparative-study of sulfide Ni-Mo catalysts, supported on gamma-Al<sub>2</sub>O<sub>3</sub> and activated carbon by using radioisotope S-35. *Bull. Soc. Chim. Belg.* **1995**, *104*, 303–309. [[CrossRef](#)]
34. Mangnus, P.J.; Bos, A.; Mouljin, J.A. Temperature-programmed reduction of oxidic and sulfidic alumina-supported NiO, WO<sub>3</sub>, and NiO-WO<sub>3</sub> catalysts. *J. Catal.* **1994**, *146*, 437–448. [[CrossRef](#)]
35. Kasztelan, S.; Wambeke, A.; Jalowiecki, L.; Grimblot, J.; Bonnelle, J.P. Site structure sensitivity of diene hydrogenation and isomerization-reactions on MoS<sub>2</sub>-gamma-Al<sub>2</sub>O<sub>3</sub> catalysts. *J. Catal.* **1990**, *124*, 12–21. [[CrossRef](#)]
36. Daage, M.; Chianelli, R.R. Structure-Function Relations in Molybdenum Sulfide Catalysts: The “Rim-Edge” Model. *J. Catal.* **1994**, *149*, 414–427. [[CrossRef](#)]
37. Sun, M.Y.; Adjaye, J.; Nelson, A.E. Theoretical investigations of the structures and properties of molybdenum-based sulfide catalysts. *Appl. Catal. A Gen.* **2004**, *263*, 131–143. [[CrossRef](#)]

38. Nogueira, A.; Znaiguia, R.; Uzio, D.; Afanasiev, P.; Berhault, G. Curved nanostructures of unsupported and Al<sub>2</sub>O<sub>3</sub>-supported MoS<sub>2</sub> catalysts: Synthesis and HDS catalytic properties. *Appl. Catal. A Gen.* **2012**, *429*, 92–105. [[CrossRef](#)]
39. Fang, K.T. The uniform design: Application of number theoretic methods in experimental design. *Acta Mathematicae Applicatae Sinica* **1980**, *3*, 363–372.
40. Wang, Y.; Fang, K.T. A note on uniform distribution and experimental design. *Kexue Tongbao* **1981**, *26*, 485–489.
41. Calais, C.; Matsubayashi, N.; Geantet, C.; Yoshimura, Y.; Shimada, H.; Nishijima, A.; Lacroix, M.; Breysse, M. Crystallite size determination of highly dispersed unsupported MoS<sub>2</sub> catalysts. *J. Catal.* **1998**, *174*, 130–141. [[CrossRef](#)]
42. Tye, C.T.; Smith, K.J. Hydrodesulfurization of dibenzothiophene over exfoliated MoS<sub>2</sub> catalyst. *Catal. Today* **2006**, *116*, 461–468. [[CrossRef](#)]
43. Wang, S.; Wang, Z.; Qin, J.; Wang, W.; Li, W.; He, D. Nanocrystalline MoS<sub>2</sub> through directional growth along the (0 0 2) crystal plane under high pressure. *Mater. Chem. Phys.* **2011**, *130*, 170–174. [[CrossRef](#)]
44. Liang, K.S.; Chianelli, R.R.; Chien, F.Z.; Moss, S.C. Structure of poorly crystalline MoS<sub>2</sub>—A modeling study. *J. Non-Cryst. Solids* **1986**, *79*, 251–273. [[CrossRef](#)]



© 2018 by the authors. Licensee MDPI, Basel, Switzerland. This article is an open access article distributed under the terms and conditions of the Creative Commons Attribution (CC BY) license (<http://creativecommons.org/licenses/by/4.0/>).